Article:

Yin, D, Peakall, J, Parsons, D et al. (4 more authors) (2016) Bedform genesis in bedrock substrates: Insights into formative processes from a new experimental approach and the importance of suspension-dominated abrasion. Geomorphology, 255. pp. 26-38. ISSN 0169-555X

https://doi.org/10.1016/j.geomorph.2015.12.008

Bedform genesis in bedrock substrates: insights into formative processes from a new experimental approach and the importance of suspension-dominated abrasion

Daowei Yin[a,b,*], Jeff Peakall[a,1], Dan Parsons[c,2], Zhongyuan Chen[b,3], Heather Macdonald[a,d,4], Paul Wignall[a,5], and Jim Best[e,6]

[a]*School of Earth and Environment, University of Leeds, Leeds, UK*

[b]*State Key Laboratory of Coastal and Estuarine Research, East China Normal University, Shanghai 200062, China*

[c]*Department of Geography, Environment and Earth Science, University of Hull, Hull, UK*

[d]*ExxonMobil Exploration Company, 222 Benmar Drive, Houston, Texas 77060, USA*

[e]*Departments of Geology, Geography and GIS, Mechanical Science and Engineering and Ven Te Chow Hydrosystems Laboratory, University of Illinois at Urbana-Champaign, Champaign, IL 61820, USA*

*Corresponding author. Tel.: +86 13671624911; E-mail: Nicholas_t_yin@hotmail.com.

[1]E-mail: J.Peakall@leeds.ac.uk.

[2]E-mail: d.parsons@hull.ac.uk.

[3]E-mail: z.chen@ecnu.edu.cn.

[4]E-mail: heathermacaverill@gmail.com.

[5]E-mail: P.B.Wignall@leeds.ac.uk.

[6]E-mail: jimbest@illinois.edu.

Abstract

Bedrock channels are common in the natural environment, and bedrock channel erosion sets the pace of denudation in many river catchments. However, in comparison to the large number of studies concerning the formation of alluvial bedforms, relatively few investigations have concerned bedrock bedform genesis. Field-based analysis of sculptured forms within bedrock channels has been restricted notably by the slow rate of bedform development in such environments. Furthermore, only a limited number of flume-scale experiments have been conducted that attempt to simulate the genesis of sculpted bedforms in bedrock channels. This study demonstrates that optimisation of clay beds through analysis of clay strength enables the development of features analogous to bedrock river channel bedforms — even at a scale that is orders of magnitude smaller than some natural examples. Three sets of suspended sediment-laden experiments were carried out using hard, medium, and soft clay bed substrates. A suite of erosive bedforms (including potholes, flutes, and furrows) developed on all experimental beds. All observed erosional features have clear equivalents to those observed in natural bedrock rivers. Bed shear strength was found to be a significant factor for the genesis of different types of simulated bedrock bedforms in our experiments with other factors, such as flow velocity, bed slope, and flow depth held approximately constant. Importantly, in a subset of experiments performed with an absence of suspended sediment, fluid flow did not result in the erosion and development of bedforms in the clay bed. Hence, this work illustrates that abrasion by suspended sediments is the key process required for the formation of these simulated

bedrock bedforms in our experiments, in the absence of bedload abrasion; other processes such as plucking, cavitation, and dissolution will have been negligible.

Keywords: Physical modelling; Bedrock bedforms; Bedrock erosion; Suspension-dominated abrasion

1. Introduction

Bedrock rivers exhibit a diverse array of erosional forms that, in turn, influence flow fields and sediment dynamics (Kor et al., 1991; Richardson and Carling, 2005; Munro-Stasiuk et al., 2009). These erosive features range in scale over at least three orders of magnitude from forms that are tens of centimetres in length to those reported to form in megafloods the width of which can reach up to 500 m (Baker and Milton, 1974; Kor et al., 1991; Herget, 2005; Richardson and Carling, 2005; Martini et al., 2009; Munro-Stasiuk et al., 2009). The genesis and formative processes of these erosional features are poorly understood and remain an area where the major knowledge gap is (Lamb et al., 2015). This omission is largely because field studies are limited by the slow rate of development of erosion within bedrock substrates and by the difficulty and danger of attempting to measure processes during infrequent high magnitude flow events in such channels (Wilson et al., 2013; Lamb et al., 2015). Physical experiments offer the opportunity to examine processes at much faster development rates and under controlled conditions (Peakall et al., 1996; Lamb et al., 2015). However, relatively few studies of erosive bedforms in substrates analogous to those observed in bedrock rivers have been conducted (Shepherd and Schumm, 1974; Wohl and

Ikeda, 1997; Carter and Anderson, 2006; Johnson and Whipple, 2007, 2010; Wilson et al., 2013; Wilson and Lavé, 2014). Furthermore, these studies have only reproduced a small number of the features identified in natural channels (Richardson and Carling, 2005). Model studies on actual rock substrates have been restricted to forming upstream facing convex surfaces (Wilson et al., 2013; Wilson and Lavé, 2014). In contrast, studies utilising artificial substrates exhibit a wider range of features, with those on weak concrete (Carter and Anderson, 2006; Johnson and Whipple, 2007, 2010) and mixed sand/mud substrates (Shepherd and Schumm, 1974; Wohl and Ikeda, 1997) producing longitudinal grooves, potholes, furrows, and step-pools. Even in these cases, experiments with initially broad erosion surfaces are dominated by longitudinal grooves that over time form ‘emergent channel geometries’ where the flow is concentrated into a single channel form (Shepherd and Schumm, 1974; Wohl and Ikeda, 1997; Finnegan et al., 2007; Johnson and Whipple, 2007, 2010; Lamb et al., 2015). Consequently, despite these advances, experiments have failed to produce the wide variety of bedforms observed in natural systems and the broad spatial distribution of these erosive features. In particular, previous experiments have failed to reproduce most kinds of flutes and hummocky forms, along with certain obstacle marks (e.g., those with reversed furrows in front of them) and various types of potholes (e.g., spiral-furrowed potholes with a spiral rib). In turn, this raises questions as to the nature of the experimental conditions and physical processes required to reproduce many of these bedrock bedforms. Here, we utilise compacted clay substrates to reproduce most of the observed features present in bedrock rivers. The nature of the formative conditions are discussed and compared to existing physical modelling and field studies. In particular, we utilise the nomenclature and typology of Richardson and Carling (2005) to compare our experiments to natural examples of bedforms formed in natural rock substrates.

1.1. Previous erosional experiments with clay beds

Although clay substrates have been used to study erosional bedforms in physical experiments, these studies produced features such as flutes and longitudinal grooves that have been compared with natural erosion in cohesive muddy substrates such as deep-sea muds and river floodplains (e.g., Dzulynski and Sanders, 1962; Dzulynski and Walton, 1963; Dzulynski, 1965, 1996; Allen, 1969, 1971). Furthermore, the applicability of these mud-rich cohesive sediments as an analogue to bedrock rivers has been questioned (e.g., Lamb et al., 2015) because of the absence of brittle fracturing that typically occurs in bedrock erosion (Engel, 1976). The majority of experiments that have been undertaken on weak muddy substrates typically used beds formed *in situ* by settling of clays in water for periods of hours to days (e.g., Dzulynski and Walton, 1963; Dzulynski, 1965, 1996; Allen, 1969, 1971), producing a range of features such as flutes and groove marks. In contrast, very little work on firm or hard mud beds has been conducted. Allen (1971) undertook a series of 13 experiments in a Perspex pipe, where particulate-flows eroded beds of kaolin-based modelling clay, producing flute-like features. Run times were between 27 and 74 minutes, although these experiments could not be continued beyond these timescales as a series of bed waves developed (Allen, 1971). Dzulynski and Sanders (1962) also used modelling clay to examine tool marks, but these experiments were undertaken by rolling objects by hand across subaerially exposed clay. Whilst these experiments on weak and firm clay beds have demonstrated a range of erosive features, quantitative data on substrate strength is absent, such as the shear strength or tensile strength and on flow properties such as basal shear stress, with which to explore the boundary conditions of such erosive features. The experiments presented here revisit the utility of clay substrates for modelling bedrock erosion, but under conditions where the substrate strength and basal shear stress are quantified, to examine the development of erosive features in the absence of brittle fracturing.

1.2. Erosive mechanisms in bedrock substrates

The major erosional mechanisms postulated to control the morphology and genesis of bedrock channels are (i) abrasion (Sharpe and Shaw, 1989; Kor et al., 1991; Sjogren and Rains, 1995; Hancock et al., 1998; Wohl, 1998; Whipple et al., 2000a; Sklar and Dietrich, 2001, 2004; Johnson and Whipple, 2007; Wilson et al., 2013; Wilson and Lavé, 2014); (ii) plucking (Baker, 1974, 1978, 1979; Baker and Komar, 1987; Sharpe and Shaw, 1989; Hancock et al., 1998; Whipple et al., 2000a, 2000b; Lamb and Fonstad, 2010; Anton et al., 2015); (iii) cavitation (Baker, 1974; Baker and Costa, 1987; Wohl, 1992, 1998; Baker and Kale, 1998; Hancock et al., 1998; Whipple et al., 2000a, 2000b); (iv) dissolution or corrosion (Sharpe and Shaw, 1989; Wohl, 1992, 1998; Whipple et al., 2000a); (v) fluid stressing (Allen, 1971; Sjogren and Rains, 1995; Richardson and Carling, 2005; Carling et al., 2009; Wilson and Lavé, 2014); and (vi) physical weathering (Sharpe and Shaw, 1989; Whipple et al., 2000a, 2000b; Carling et al., 2009). Of these, abrasion and plucking are considered the most important processes, with plucking effective when rocks are fractured and exhibit discontinuities, whilst abrasion is thought to dominate in massive rock with weak jointing (Hancock et al., 1998; Whipple et al., 2000a; Chatanantavet and Parker, 2009; Lamb and Fonstad, 2010). Abrasion can occur as a result of traction load, saltating bedload, or as suspended-load — with debate on the relative efficacy of these three modes in bedrock rivers (Lowe, 1979; Hancock et al., 1998; Whipple et al., 2000a). Evidence for the importance of cavitation in the field and experiments is lacking, although theoretically it is thought to be a plausible contributing factor (Whipple et al., 2000a; Carling et al., 2009). Weathering of bedrock through corrosion, physical frost weathering, and chemical weathering may also be important but has been little studied (Büdel, 1982; Lamb and Fonstad, 2010; Pelletier and Baker, 2011).

2. Methodology

A series of four experimental runs were undertaken to examine the nature of erosion in clay beds by open channel flow, three containing a particulate load of fine-grained sand (silica sand with a d_{10} of 82 μm, d_{50} of 143 μm, and d_{90} of 245 μm) and one without particulate load (clear water). Air-dried modelling clay (Potter's Scola Clay) was used as the substrate, with the initial undrained shear strength of the clay beds adjusted between runs through presoaking of the clay bed.

2.1. Experimental setup

The experiments were conducted in the Sorby Environmental Fluid Dynamics Laboratory (SEFDL) in the School of Earth and Environment, University of Leeds. An 8.75-m long, tilting, recirculating hydraulic slurry flume (0.30 m wide by 0.30 m deep) was used for the experiments (Fig. 1). The flume contained a false floor into which a tray (0.90 m long and 0.075 m deep) containing the clay bed could be inserted, such that the upper surface of the clay bed was flush with the false floor (Fig. 1). The water depth was set to 0.14 m above the clay bed in all experiments, and uniform flow was obtained by adjusting the flume slope to 0.005. An array of ten 4 MHz ultrasonic Doppler velocimetry probes (UDVP; Best et al., 2001) were positioned downstream of the clay bed, pointing upstream, with the ends of the transducers positioned level with the end of the clay bed (Fig. 1). The UDVP collected data for 99 seconds at a temporal resolution of 8 Hz; the operating parameters for the UDVP are shown in Table 1. The UDVP probes enabled flow velocity profiles, initial basal shear stress (Exp. 1: $\tau \approx 3.1$ Nm^{-2}; Exp. 2: $\tau \approx 4.8$ Nm^{-2}; no data for Exp. 3 but of similar order to experiments 1 and 2), and mean flow velocity (u_{mean} = 0.75-0.81 ms^{-1}) to be measured above the clay bed. These data allow calculation of the Froude number (Fr = 0.64-0.69) (Table 2). Three experiments were undertaken with a suspended sediment load (Exps. 1-3). A further experiment (Exp. 4) was run for 720 min without sediment load, with undrained shear strength of 10.5 kPa, initial basal shear stress of 3.1 Nm^{-2}, and flow velocity of ~0.81 ms^{-1} (Fr = ~0.69). Water temperature during the experiments varied between 8 and 12°C. The experiments undertaken herein altered substrate resistance between runs and examined the role of suspended sediment; whilst slope, water depth, initial flow velocity, and discharge were held approximately constant.

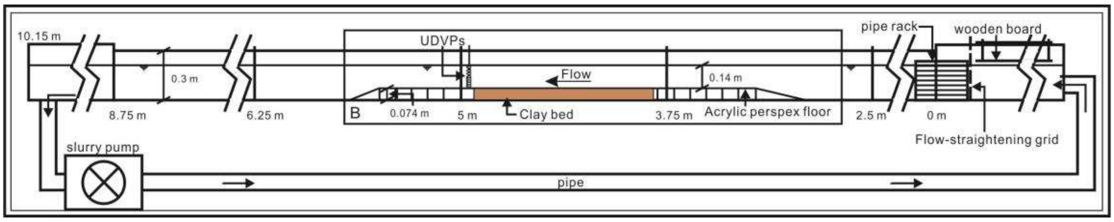

Fig. 1 Schematic drawing of the current experimental setup of the hydraulic slurry flume. The dark area represents the clay bed with a tray that was lowered into position so that the top surface of the clay bed was flush with the surrounding false floor.

Table 1

Parameters for the UDVP used in the current experiments

Ultrasonic frequency	Bin width	Bin distance	Measurement window	Number of bins	Multiplexing time delay	Number of profiles per transducer	Ultrasound velocity	Transducer diameter	Bins for analysis
4 MHz	1.48 mm	0.74 mm	5-101.2 mm	128	15 ms	500	1480 ms^{-1}	8 mm	31-38

Table 2

The hydraulic parameters of the experiments

Flow depth (m)	0.14
Bed slope	0.005
Mean velocity (u_{mean}) (ms^{-1})	0.75-0.81
Temperature (T) (°C)	8-12

Grain size (d) (µm)	D_{10}: 82 D_{50}: 143 D_{90}: 245
Froude number (Fr)	0.64-0.69
Flow Reynolds number (Re)	84635-91406
Impact Stokes number (St)	for d_{50}: 27 for d_{90}: 47
Initial basal shear stresses (τ) (Nm^{-2})	Exp. 1: 3.1 Exp. 2: 4.8

2.2. Clay preparation and undrained shear strength measurement

Air-dried modelling clay (Potter's Scola Clay) was used as the substrate and consisted primarily of illite-smectite, kaolinite, and quartz (Table 3). The dissolution of these materials in water under laboratory conditions (clear tap water with water temperature of 8-12°C), will be negligible (Huang and Keller, 1971). The beds were soaked in clear water prior to each run, with this presoaking time being altered to adjust the initial undrained shear strength of the substrate from 10.5 kPa (Exp. 1), through 7.5 kPa (Exp. 2) to 5.5 kPa (Exp. 3) (Fig. 2) — referred to herein as hard, medium, and soft. Shear strength was measured using a hand shear vane meter with a four-blade vane (25.4 mm wide by 50.8 mm deep). After soaking to the required strength, the clay was placed in a tray and inserted into the flume. In order to ensure the original bed surface was flat, the clay surface was smoothed by hand using a metal board to the same level as the surrounding Perspex floor.

Table 3

X-ray diffraction analysis for composition of modelling clay used in the experiments

	Quartz	Illite-smectite	Kaolinite	Hematite
Chemical composition (%)	35.3	39.1	21.1	4.5

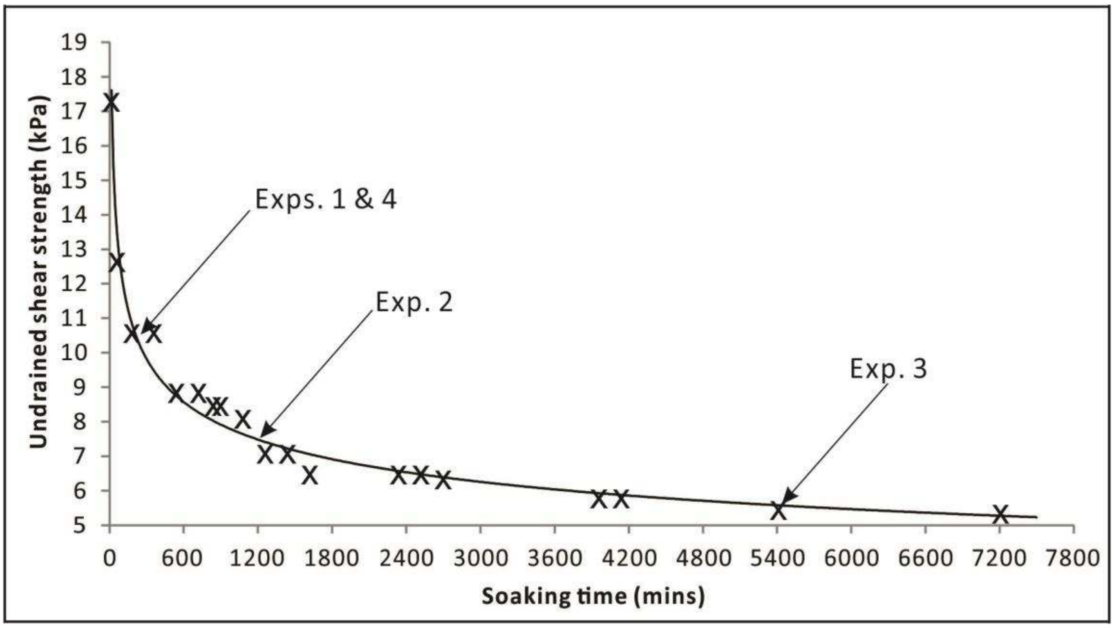

Fig. 2 Variation in undrained shear strength with soaking time. Positions of the initial undrained shear strengths are shown for each experiment; Exps. 1 & 4: hard: 10.5 kPa; Exp. 2: medium: 7.5 kPa; Exp. 3: soft: 5.5 kPa.

2.3. Experimental conditions

Experiments were initiated with smooth clay beds (Exps. 2 and 3) and with a number of circular bed defects (Exp. 1; Fig. 3). The defects consisted of five holes 2.4 cm in diameter and 0.3 cm in depth, two medium-sized hollows 0.9 cm in diameter and 0.2 cm in depth, and two smaller holes 0.6 cm in diameter and 0.2 cm in depth (Exp. 1; Fig. 3). Silica sand with a d_{10} of 82 µm, d_{50} of 143 µm, and d_{90} of 245 µm was added to the flow. In order to maintain a constant sediment supply, 1.5 kg of sand was progressively introduced every 15 min, thus compensating for sediment slowly accumulating within the pipework of the hydraulic flume. Sediment concentration was monitored via water samples collected at a depth of ~7 cm above the Perspex floor and ~10 cm downstream of the clay beds every 20 min; 95% of all SSC measurements were in the range of 0.10% to 0.20% by weight. Notably, the eroded clay was also recirculated within the flume; however, this makes a very minor contribution to the suspended sediment concentration because the total volume of clay eroded is small. The Rouse number, *Z*, is calculated to provide an estimation of the transport condition of particles within a flow:

$$Z = \frac{W_S}{kU_*} \qquad (1)$$

where W_s is the sediment fall velocity, calculated here using the expression of Gibbs et al. (1971), k is von Karman's constant taken as 0.4, and U_* is the shear velocity. For our experiments, Rouse numbers were ~0.4-0.6 for the d_{50} of 143 µm and ~1 for the d_{90} of 245 µm.

The impact Stokes number, *St*, is also calculated. The *St* characterises particles impacting a wall, with larger particles rebounding whilst particles below a certain size are viscously damped.

$$St = \frac{\rho_s U_i D}{9\mu} \qquad (2)$$

where ρ_s is sediment density, U_i is particle impact velocity, D is grain diameter, and μ is dynamic fluid viscosity (e.g., Lamb et al., 2015). For saltating grains the particle impact velocity is calculated using the equation proposed by Wiberg and Smith (1985); however, expressions are not available for suspended load particle impact velocity. Here we take the impact velocity as the vector sum of the mean downstream velocity and the fall velocity; the latter calculated using the expression of Gibbs et al. (1971). This yields impact Stokes numbers of ~27 for the d_{50} and ~47 for the d_{90} particle sizes.

Each experiment was then run until no further morphological change of the clay bed was observed, in part corresponding with the substrate beginning to be covered by sand deposited from suspension. This deposition of sand at the end of the runs occurred because of the progressive erosion and lowering of the clay bed, resulting in the clay surface being lower than the surrounding Perspex floor, leading to progressive trapping of sediment. The total run times of experiments 1-3 (hard, medium, soft) were 1680, 1800, and 1080 min, respectively. The experiments were stopped periodically in order to take photographs after slowly draining the flume (e.g., Fig. 3B). In addition, the bathymetry of the experimental substrates was scanned using a SeaTek Ultrasonic ranging system consisting of 12 transducers operating at 5 MHz in order to measure the erosive amount/rate and the depth of the erosional features. These breaks in each experimental run took place at 60 and 120 min and then every 120 min until the end of the experiment, with an additional sampling point at 30 min for experiment 1. In order to rectify the distorted photographs, four straight control bars with 10 control points on each of them were distributed around the edges of the clay bed and corrections were undertaken using DxO ViewPoint software.

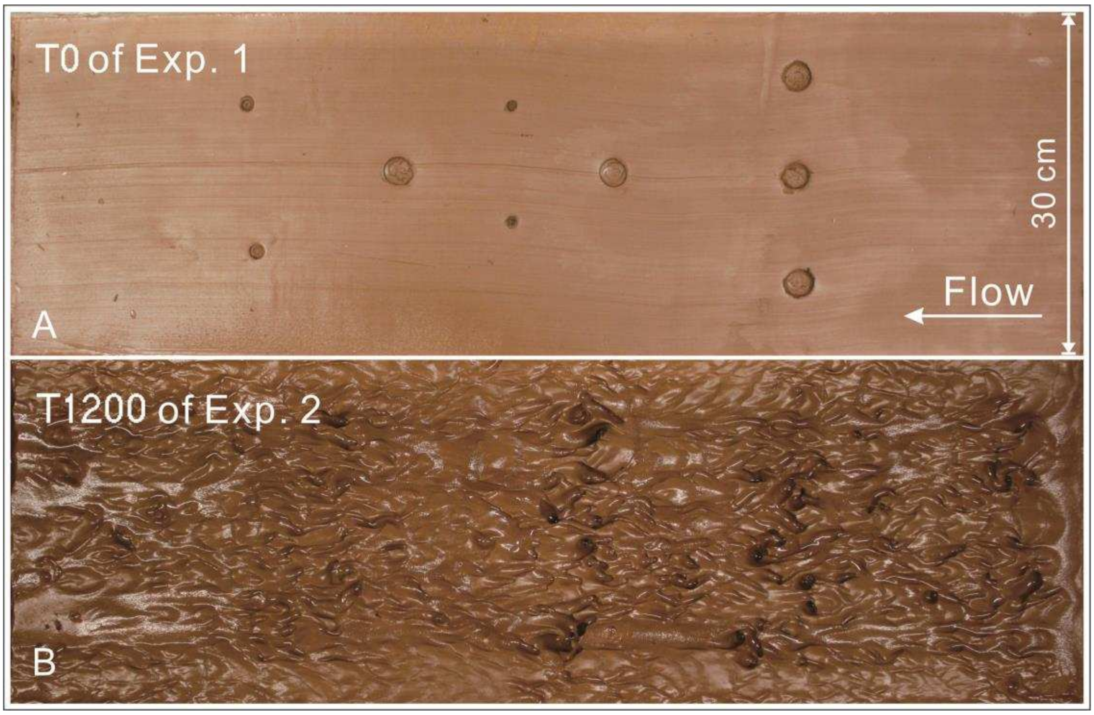

Fig. 3 (A) The initial experimental bed of Exp. 1: hard, the preformed larger holes are 2.4 cm in diameter and 0.3 cm in depth; the medium-sized hollows are 0.9 cm in diameter and 0.2 cm in depth, and the smallest hollows are 0.6 cm in diameter and 0.2 cm in depth. (B) The fully developed experimental bed of Exp. 2 after 1200 min run time. The initial bed of Exp. 2 was a flat bed without hollows. Flow was from right to left in both cases.

3. Results

3.1. Clear water experiment

The experiment undertaken without sediment load or bed defects (Exp. 4) and run over 720 min exhibited no bed erosion. The lack of erosion was confirmed by the absence of discolouration of the water in the flume channel by clay.

3.2. Evolution of the clay bed

The evolution and erosion rate of the clay bed differed between the three experiments with a suspended-load (Exps. 1-3) as a function of the undrained shear stress. For the hard clay bed (Exp. 1: 10.5 kPa), the bed barely altered until after 960 min and stopped eroding after 1440 min, whilst for the medium bed (Exp.2: 7.5 kPa) bedforms initiated after 720 min and stopped eroding after 1320 min. The erosion of the softest experimental bed (Exp. 3: 5.5 kPa) began after 480 min and ended at 960 min, although this run was initiated with a series of bed defects restricting direct temporal comparison. Whilst bedform development occurred at different rates in experiments 1-3, the final forms in each showed strong similarities, with the three experiments producing an array of erosional features. Details of the most common types and geometries of these erosional features (including four types of potholes, three types of flutes, two types of furrows, and two types of convex and undulating bedforms) are given below together with a comparison with natural bedrock sculpted forms.

3.3. Individual simulated erosional bedrock bedforms

3.3.1. Potholes

Potholes are one of the most evident abrasion sculpture forms in bedrock channels (Elston, 1917, 1918; Alexander, 1932; Maxson and Campbell, 1935; Ives, 1948; Allen, 1971, 1982; Kor et al., 1991; Wohl, 1992, 1993; Zen and Prestegaard, 1994; Wohl and Ikeda, 1998; Richardson and Carling, 2005; Munro-Stasiuk et al., 2009) as well as the most commonly observed erosional features on the experimental clay beds. The potholes observed in the present experiments can be classified into the following categories of Richardson and Carling (2005): (i) simple potholes; (ii) potholes with extended exit furrows s; (iii) open potholes; (iv) spiral-furrowed potholes with a spiral rib; (v) spiral furrowed pothole; (vi) potholes with entry and extended exit furrows; (vii) potholes with exit furrows; (viii) potholes with horizontal furrows; (ix) potholes with lateral external secondary furrows; (x) complex potholes / convoluted potholes; and (xi) hierarchical potholes. Importantly, potholes representing all 11 categories were observed. For brevity, only the details of the four most common types of potholes are described herein (Fig. 4). Extensive discussion of all the features observed is provided by Yin (2013).

Simple Potholes: This kind of isolated, quasi-round pothole with a cylindrical form is common in natural bedrock channels and was common in the current experiments (Figs. 4A1, A2; note that dimensions of features are provided in the figures). Simple potholes could be observed on the bed as part of more complex features or sometimes in the early stage of the experiments. These potholes typically evolved into other forms (e.g., flutes and short furrows), widening and deepening their quasi-round opening, and thus were rarely stable over the duration of the experiments. The radius of the opening was usually slightly larger than that of the internal radius of its base, but the form is still regarded as approximately cylindrical. The diameter of the opening enlarged with time and extended in a specific direction, usually downstream, to form exit furrows. As a consequence, the rims of solitary potholes typically did not maintain a quasi-round geometry.

Potholes With Extended Exit Furrows： Potholes with extended exit furrows were the most common pothole developed in the experimental beds (Figs. 4B1 to B4). The downstream ends of the exit furrows were not always closed, and the lengths of the exit furrows were much bigger than the diameters of the primary potholes. The ratio of length to diameter ranges from 3.1 to 4.5 in the experiments conducted. The exit furrows usually exhibited a curved planform profile in the downstream direction with lengths more than twice as long as the widths. These features were still considered potholes because they developed from individual hollows located at the upstream end that are much deeper than the rest of the bedforms. The rims of these exit furrows were parallel, and in some cases they were closed at their downstream end (Figs. 4B1, B2). In other cases, the exit furrows were totally open at their downstream ends (Figs. 4B3, B4). Individual simple potholes could develop in time into potholes with extended exit furrows, or open potholes, if they did not connect to adjacent bedforms.

Open Potholes： Open potholes were defined as a pothole that has an open end in planview (Figs. 4C1, C2) that is almost as wide as the diameter of the primary hollow. These open potholes usually lack a lee side edge and have an entire open end; the dominant orientation is in the downstream direction. On some occasions, their upstream end rims were not closed, and they could be eroded by other marks in front of them, for example when an entry furrow developed.

Spiral-furrowed Potholes With A Spiral Rib： On the experimental clay beds, many of the erosional marks had entry spiral ribs (e.g., (Figs. 4D1 to D3) that are widely observed in natural bedrock channels (Alexander, 1932; Ängeby, 1951; Allen, 1982; Jennings, 1983; Baker and Pickup, 1987; Wohl, 1992; Kor and Cowell, 1998; Richardson and Carling, 2005). The spiral rib is a small curved part extending in the upstream direction adjacent to the upstream rim of a pothole. The head of the spiral rib was usually cuspate or approximately cuspate and pointed predominantly in the upstream direction. The length and width of the spiral rib was normally far less than the primary pothole with which it was connected. The length of the spiral rib is normally no greater than one third of the diameter of the primary pothole. Sometimes, near the top open rim of potholes, a secondary lateral furrow extends from the rib, with cuspate rims forming on the inner wall of the pothole (Fig. 4D2).

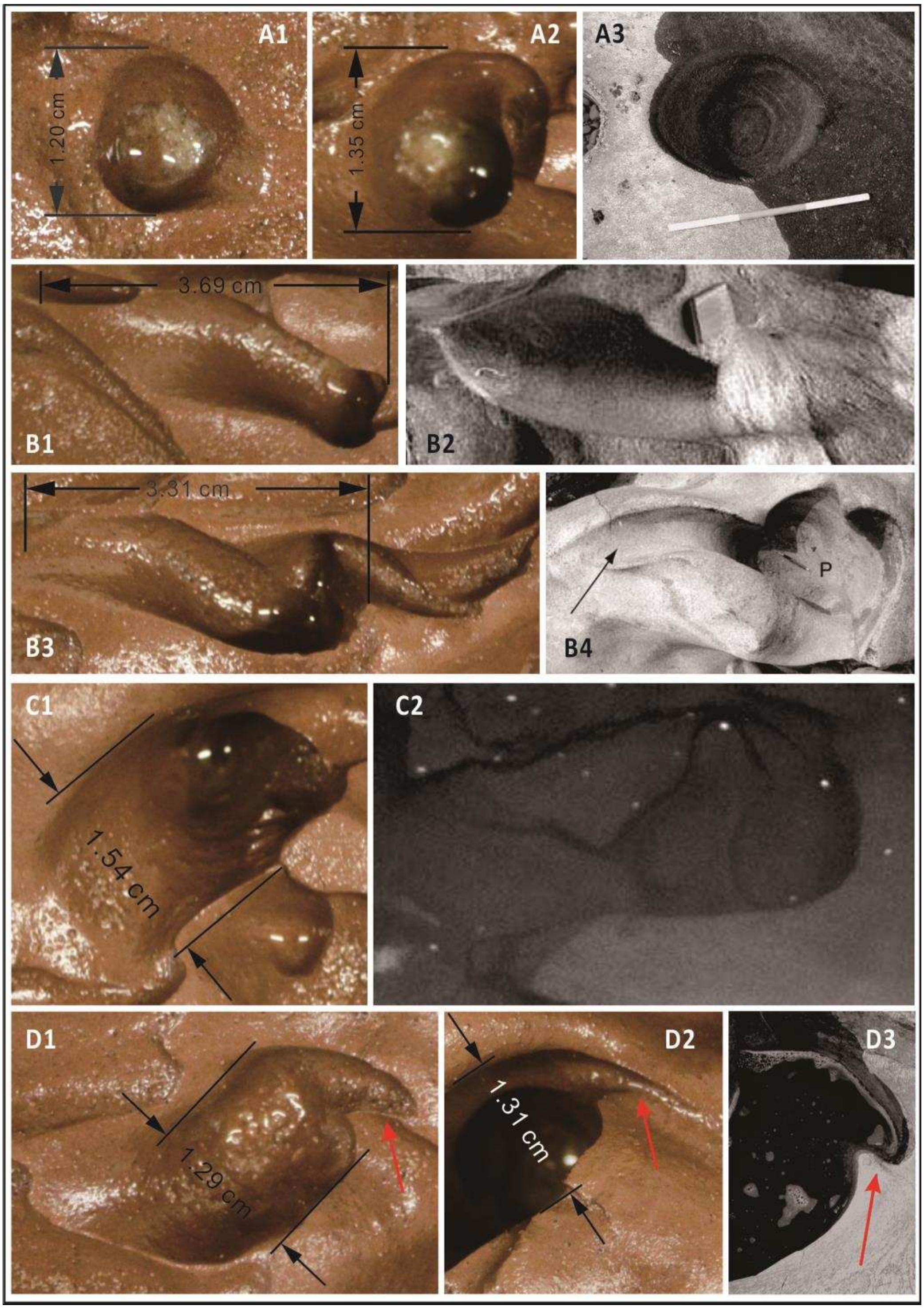

Fig. 4 Morphology of potholes in the experiments and in bedrock channels. Unless mentioned otherwise flow is from right to left. (1) Simple potholes: A1 and A2 from Exp. 2. A3 shows a simple pothole in fine-grained sandstone from the River Lune (Halton), UK (from Richardson and Carling, 2005). The scale bar in A3 is 0.6 m long. (2) Potholes with extended

exit furrows: The exit furrows of this kind of pothole were much longer than in potholes with an entry furrow. B1 and B3 from Exp. 2. B2 and B4 are two examples from the field (from Richardson and Carling, 2005). In B2, the notebook is 0.15 m long. B3 and B4 illustrate compound potholes with extended exit furrows. See pen (P) in B4 for scale, flow from top right to bottom left in B4. (3) Open potholes: C1 from Exp. 2. C2 is from the River Lune (Halton), UK. It is 1.20 m long with a diameter of 0.60 m (from Richardson and Carling, 2005). (4) Spiral-furrowed pothole with a spiral rib: the examples in D1 and D2 were observed in the central part of the bed in Exp. 2. D3 shows a natural example observed in Woolshed Creek, Australia. The pothole is ~1.5 m across in its short dimension (from Richardson and Carling, 2005). The arrow points to the spiral ribs of the potholes in D3. A3, B2, B4, C2, and D3 are reprinted from Richardson and Carling (2005) with permission from GSA.

3.3.2. Longitudinal features

Besides potholes, another principal type of erosional mark in bedrock channels are longitudinal features, commonly flutes and furrows (King, 1927; Allen, 1971, 1982; Kor et al., 1991; Wohl, 1992, 1993; Tinkler, 1997a; Hancock et al., 1998; Richardson and Carling, 2005). Flutes and furrows are relatively shallow compared with potholes, with their depth usually being much smaller than their length (Richardson and Carling, 2005). In our experiments the average depth of the flutes was 0.82 cm compared with an average depth of 1.93 cm for the potholes (Appendix 1).

Flutes： Flutes are a common form typical of erosive bedforms in bedrock channels (Maxson and Campbell, 1935; Allen, 1971; Kor et al., 1991; Tinkler, 1993; Baker and Kale, 1998; Hancock et al., 1998; Whipple et al., 2000b; Richardson and Carling, 2005; Munro-Stasiuk et al., 2009). The experimental approach herein produced various types of flutes that are almost identical with flutes present in natural bedrock channels (Fig. 5).

Deep Flutes： Deep flutes have been defined as those whose depth are >25% of their length (Richardson and Carling, 2005). Figures 5A1 and 5A2 show deep flutes in our experimental substrate and those from a natural bedrock channel, respectively, illustrating that they are almost identical with both having a similar internal structure.

Flutes With Internal Secondary Structure： Flutes with internal secondary structures (Allen, 1971) formed in the experiments and show strong similarities to flutes formed in many bedrock substrates (Figs. 5A1 and 5A2; Richardson and Carling, 2005). However, this type of flute was not as common as flutes with external secondary structures in the flume experiments. This may, in part, be because the scale of flutes in the present experiments was too small to contain visible smaller internal secondary structures (Figs. 5B1 and B2).

Flutes with external secondary structure： Most of the flutes in these experiments were classified as flutes with external secondary structures, formed outside the primary flutes (Figs. 5C1 to C5). Previous studies have indicated that flutes with external secondary structures may be caused by a discontinuity in the substrate (Hancock et al., 1998; Richardson and Carling, 2005). However, the clay beds used herein were well mixed and essentially homogenous and therefore lacked any significant discontinuities. Additionally, the size of these features in the clay bed was variable, with some as large as, or only slightly smaller, than the primary flutes; whilst others were much smaller than the primary flutes. The ratio of the length of the secondary structures and the primary flutes ranges from 0.7 to 0.9 (Figs. 5C1 to C4).

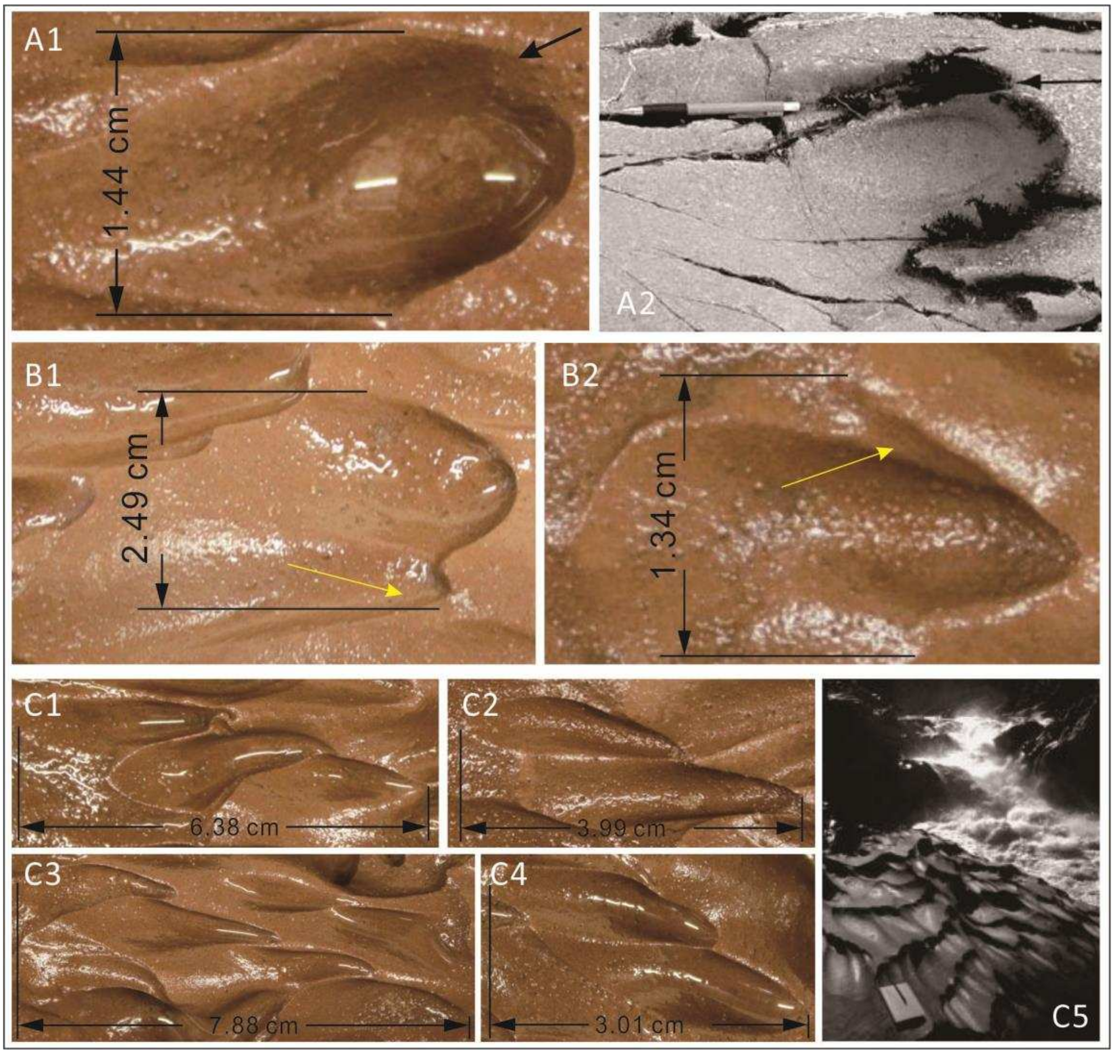

Fig. 5 Flutes. Unless mentioned otherwise flow is from right to left in all cases. (1) Deep flutes: A1: deep flute in Exp. 1; A2: deep flute in the Borrow Beck, UK (from Richardson and Carling, 2005, pen for scale). Both A1 and A2 contain internal secondary flutes close to their upper rims (black arrows). (2) Shallow flutes with internal secondary structure: B1 and B2 show flutes with internal secondary furrows on one side of their flanks, Exp. 2 (arrowed). (3)

Flutes with external secondary structures: C1 to C4 demonstrate several rows of flutes developing in Exp. 2. Normally the first flute in a row (the rightmost flute) was regarded as the primary flute, with the remaining flutes defined as secondary. C5 shows a row of rhythmic fine flutes and ripples from the Indus River near Nanga Parbat, Pakistan; notebook measures 12 × 19 cm for scale (from Whipple et al., 2000a). Flow from top left to bottom right. A2 and C5 are reprinted from Richardson and Carling (2005), and C5 is reprinted from Whipple et al. (2000a) with permission from GSA.

Longitudinal furrows: Furrows are also a common longitudinal abrasion feature in bedrock channels (Fig. 6). According to the definition of a typical furrow, the distal end should be the mirror image of its proximal end (Wohl, 1993; Wohl and Achyuthan, 2002; Richardson and Carling, 2005). The key difference between furrows and flutes is that furrows are almost symmetrical in cross-sectional and in longitudinal profile. The experimental beds demonstrated the development of most types of furrow that have been observed in the field (Fig. 6).

Short furrows usually have closed elliptical rims in planview (Figs. 6A1 to A4), with their depth being no more than a quarter of their length (Richardson and Carling, 2005). Typically, the average depth of furrows in our experiments was 1.37 cm and therefore not as deep as potholes (average depth: 1.93 cm), although potholes are sometimes elliptical in planform. The cross section of a short furrow is a 'U' shape, with the inner walls and bottom of the furrow usually being smooth (Richardson and Carling, 2005).

Sinuous parallel-sided furrows: The lengths of sinuous parallel-sided furrows ranged from 1 (1.3 cm) to >10 cm (16.2 cm) (Figs. 6B1, B2, B4), with their dominant orientation being longitudinal, with either proximal or distal ends that curved away from the flow direction. The rims of these furrows were mostly parallel, with their ends being either open or closed, the slope of both ends being gentle, and the rims being either round or cuspate. The walls and the bottom of these furrows were usually smooth without secondary structures or defects. Some long sinuous furrows developed from the connection of curved or sinuous short furrows, and therefore the depth of the furrows was not always uniform. Overall, the morphology of these furrows was similar to field examples (Fig. 6B2).

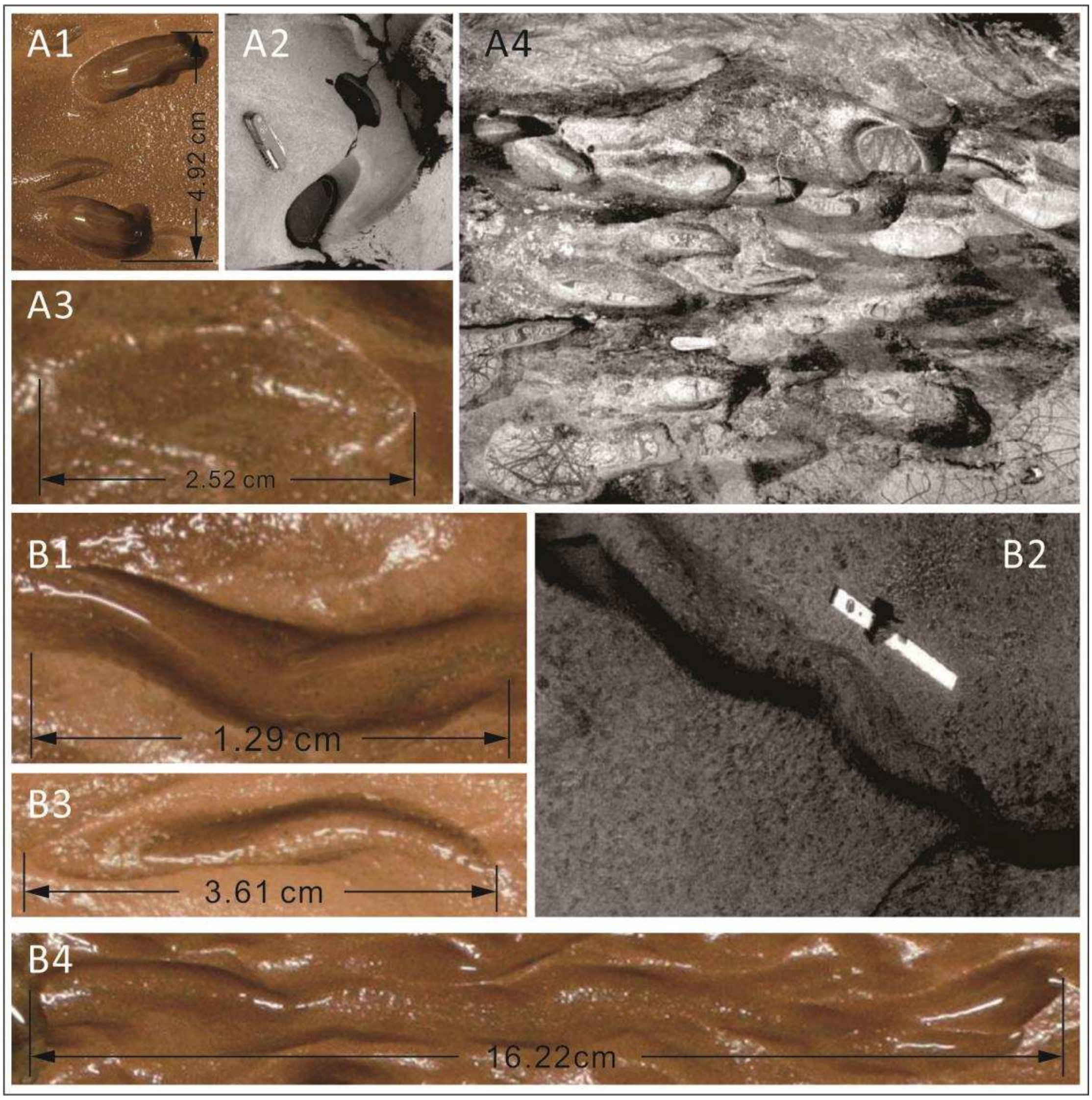

Fig. 6 Longitudinal furrows. Unless mentioned otherwise flow is from right to left. (1) Straight short furrows: A1 and A3 are straight short furrows in Exp. 2. A2 and A4 are field examples from the River Dee, UK; penknife in A2 and A4 (white) for scale (from Richardson and Carling, 2005). (2) Sinuous parallel-sided furrows: B1, B3, and B4: examples of features observed in Exp. 3, 2, and 1, respectively. B2 was observed in the River Lune (Halton), UK; the scale is 0.60 m long. Flow from bottom right corner to top left corner. A2, A4, and B2 are reprinted from Richardson and Carling (2005) with permission from GSA.

3.3.3. Convex and undulating surfaces

A number of convex and undulating surfaces also formed in the experiments, with hummocky forms being the most common type within this category (Richardson and Carling, 2005). The most common kind of hummocky form was a sharp-crested hummocky morphology, which resembles ripples and dunes found in cohesionless substrates, but possessed more obvious sharp crests (Figs. 7A1 to A3). This morphology has led to these features being termed: pseudo-ripples and pseudo-dunes (Richardson and Carling, 2005), eversion marks (Ängeby, 1951), hummocky surfaces (Whipple et al., 2000b), or ripple-like bedforms (Hancock et al., 1998; Whipple et al., 2000a) in previous studies.

Sharp-crested hummocky forms: The sharp crests of these features developed nonlongitudinally and divided the convex form into two parts, having a stoss side and a lee side (Fig. 7A1). The slope of the lee side (slope = 0.65) was often steeper than that of the stoss side (slope = 0.27). In the experiments, the sinuous crests were parallel to each other, and the form of the convex parts was similar. The convex forms were arranged in rows with regular spacing and orientation parallel to the flow direction (Figs. 7A1, A2), thereby producing regular trains of sharp-crested hummocky forms (Richardson and Carling, 2005).

Obstacle marks: Obstacle marks (Figs. 7B1 to B5) are the other typical composite erosional morphology found in the field (Baker, 1974; Sharpe and Shaw, 1989; Kor et al., 1991; Lorenc et al., 1994; Herget, 2005; Richardson and Carling, 2005; Munro-Stasiuk et al., 2009; Euler and Herget, 2012; Herget et al., 2013), and they were also commonly developed on all three experimental beds. In the field, obstacle marks are scour marks caused by flow separation and the horseshoe 'junction' vortex generated when flow encounters an obstacle

(Simpson, 2001). These obstacles may consist of nontransported boulders; however, in general the obstacle is a projecting part of the substrate and is an integral part of the obstacle mark (Richardson and Carling, 2005). These obstacle marks possess a crescentic planform shape (Allen, 1982), and in the present experiments they consisted of a raised projection as an obstacle with average width of 0.9 cm and a crescentic reversed furrow (average depth: 1.7 cm) upstream of it. The crescentic reversed furrows were parallel-sided in planview with either open or closed ends.

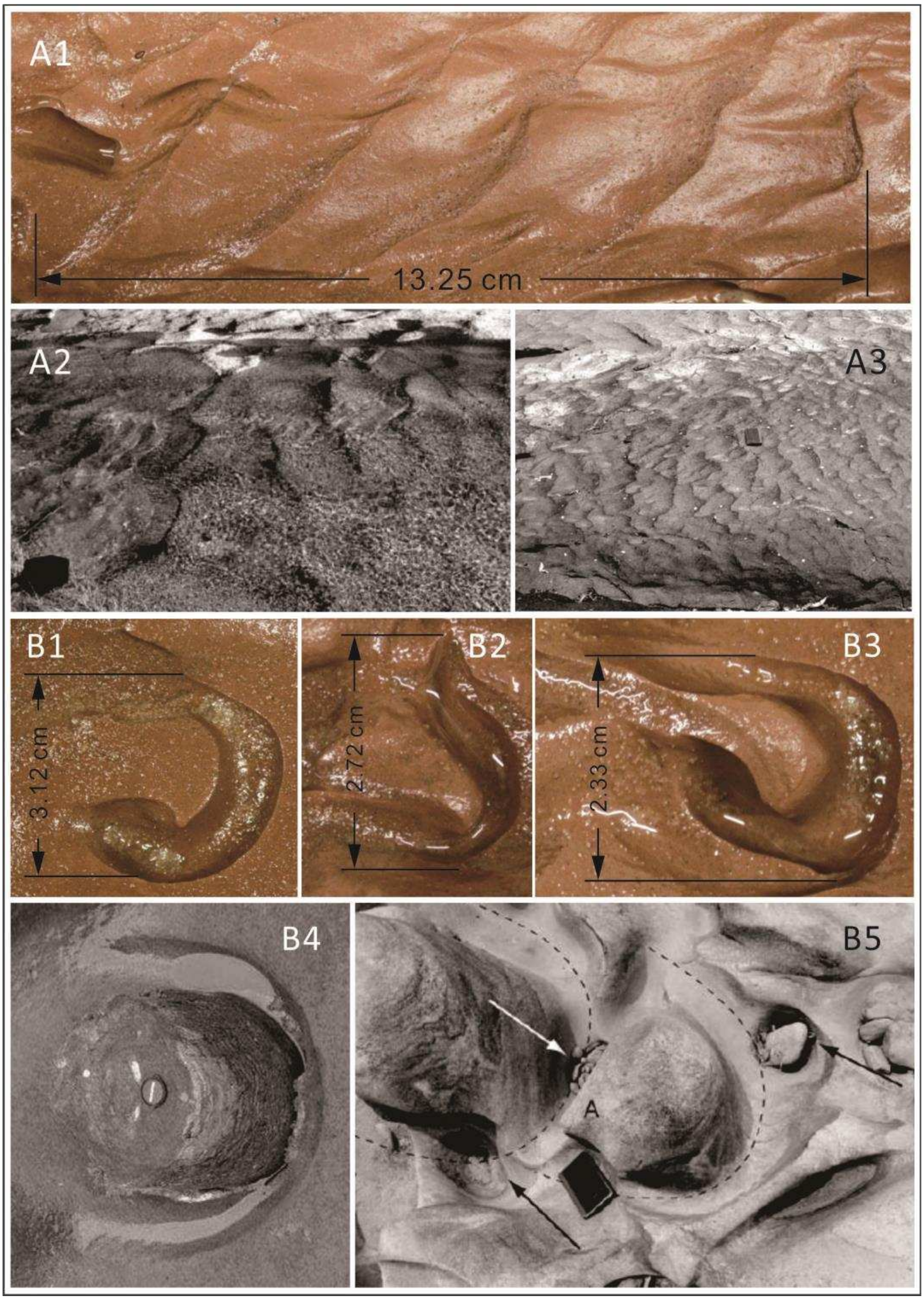

Fig. 7 (1) Hummocky forms: A1: regular trains of sharp-crested hummocky forms observed in Exp. 2. A2 and A3: hummocky forms found in natural bedrock surfaces; camera bag at the bottom left corner of A2, 0.20 m across, and a 0.15 m long handbook in A3 for scale (from Richardson and Carling, 2005). (2) Obstacle marks: B1 and B2 are observed in Exp. 1, and B3

is in Exp. 2. B4 and B5: obstacle marks observed in the field; the lens cap in B4 and the 0.15-m-long notebook in B5 for scale (from Richardson and Carling, 2005). Flow from right to left in all cases. A2, A3, B4, and B5 are reprinted from Richardson and Carling (2005) with permission from GSA.

4. Discussion

The three sediment-laden experiments described herein, using modelling clay as the bed substrate with different initial shear strengths, produced a wide array of erosive bedforms that closely replicate many features observed in natural bedrock river substrates. This included replicating 7 kinds of potholes, 9 kinds of flutes, 15 kinds of furrows, and 4 examples of other bedforms (Appendix 1; Yin, 2013); of these, the main bedform types have been illustrated herein. The degree of similarity is so strong that the morphology of many of the bedforms in the clay bed was almost identical to examples observed in the field (Figs. 4-7), this despite the scale of the laboratory experiments, which is orders of magnitude smaller than some natural examples. All of the forms were observed to originate on both flat beds and on a bed with initial defects, suggesting that initial negative defects on the surface of bedrock are not critical for the genesis of bedforms or for the overall variety of erosional forms. However, the imposed defects were observed to alter the specific type of bedform because obstacle marks formed more frequently in the vicinity of the imposed defects; protrusions formed between pairs of furrows generated from the flanks of adjacent negative defects (Fig. 7). Whilst the present experiments reproduced the majority of the different bedforms recognised by Richardson and Carling (2005), a number of bedforms identified by these authors were not observed in our experiments (Appendix). Some of the missing features may be related to heterogeneities in natural substrates that were not present in the experiments. In addition, lateral features (bedforms carved into vertical or subvertical faces on the sides of channels) were not observed in the present experiments as all experiments utilised a flat bed. If the lack of substrate heterogeneity and lack of lateral topography in the experiments is taken into account, then a remarkable range of forms observed in natural bedrock substrates were observed in the experiments.

Although all three experiments produced many types of erosional forms, some differences in the diversity of forms were seen between the different substrates (number of types: Exp. 1: 11; Exp. 2: 29; and Exp. 3: 6; Appendix), with experiment 2 (medium hard bed) showing the greatest diversity of forms. In the absence of repeat runs, the degree of variation between runs with nominally identical conditions cannot be quantified. Nonetheless, the present experiments suggest that the given type of modelling clay — initial undrained shear strength of 7.5 kPa and a shear flow with initial basal shear stress of 4.8 Nm^{-2} — appears to provide excellent characteristics for an analogue bedrock substrate for creating erosional bedforms.

In the present experiments, erosion is concentrated within the erosional features (the negative defects of the potholes, flutes, furrows, etc.), widening and deepening them with time; whilst the areas between the bedforms have far less erosion. The uniform cohesive substrate is unaffected by plucking processes; and similarly dissolution, corrosion, and cavitation are either not present or negligible given the materials and timescales of the experiments. As a consequence, erosion is overwhelmingly caused by abrasion from the suspended particulate load. This was confirmed by the initial clear water run where no features were formed. The concentration of erosion on the downstream side of bedforms suggests that the abrasion is caused by suspended load because it is closely coupled to flow dynamics rather than being caused by bedload saltation; the latter has been found to erode preferentially the upstream parts of bed protuberances (Whipple et al., 2000a). For the experiments herein, Rouse numbers, Z, were ~0.4-0.6 for the d_{50} of 143 μm and ~1 for the d_{90} of 245 μm and thus well below the suspension threshold of $Z < 2.4$ (e.g., Lamb et al., 2015), confirming that even the coarsest material was in suspension.

Impact Stokes numbers, St, for the experiments range from ~27 for the d_{50} and ~47 for the D_{90} particle sizes. Previous work has shown that particles below St of ~10-20 exhibit viscous damping (Joseph et al., 2001; Ruiz-Angulo and Hunt, 2010; Li et al., 2012), whilst numeric modelling of erosion from bedrock rivers has used $St = 30$ (Lamb et al., 2008) or 75 (Scheingross et al., 2014) to define the extent of viscous damping and the position at which erosion drops to zero. The calculated Stokes numbers in the experiments (Table 2) are therefore in agreement with measurements and theory from individual grain collisions but are less than the value used in the modelling of bedload erosion by Scheingross et al. (2014). The critical Stokes range is a weak function of the elasticity of the impacting particles and the substrate (Davis et al., 2002). The present experiments use a clay bed that likely exhibits a different elasticity to weak concrete or bedrock, though the Youngs modulus of the material is unknown; this may account for the observed differences between the present experiments and numerical models of bedrock erosion (Scheingross et al., 2014; Lamb et al., 2015).

The present experiments are also the first to reproduce large surfaces composed of arrays of different and varied bedrock bedforms and in marked contrast to previous experiments that tended to form a narrow range of features prior to formation of a single 'emergent channel' (Shepherd and Schumm, 1974; Wohl and Ikeda, 1997; Finnegan et al., 2007; Johnson and Whipple, 2007, 2010; Lamb et al., 2015). In part, this may reflect differences in initial conditions. Some previous experiments started with an initial channel (Shepherd and Schumm, 1974; Finnegan et al., 2007) or with the centre being lower than the edges (Johnson and Whipple, 2010), which will both encourage channelization. Other experiments possessed very shallow flow depths (0.02-0.03 m) that may have restricted macroturbulence and bedform development (Wohl and Ikeda, 1997). However, the experiments of Johnson and Whipple (2007) did start with initial planar bed conditions and greater flow depths (0.06-0.09 m), but still produced emergent channel geometries. A major difference between the present experiments and those of Johnson and Whipple (2007) is that the latter experiments were dominated by saltation-driven abrasion, rather than suspension-driven abrasion. This is reflected in Rouse numbers of 18-67 for the d_{50} of 2.5 mm and 24-90 for the d_{90} of 3.76 mm based on Table 1 from Johnson and Whipple (2007) and calculating fall velocities with Gibbs et al. (1971). Other experiments have largely been undertaken with dominantly saltation-driven abrasion as reflected in their Rouse numbers, Z ~ 2.3-6.2, with suspension-dominated abrasion only beginning to occur as narrower channels emerged (Wohl and Ikeda, 1997; Finnegan et al., 2007; Johnson and Whipple, 2007, 2010). A second important difference is that the present experiments were in the subcritical flow regime, Fr ~ 0.6-0.7 in contrast to previously published experiments that were mostly strongly supercritical, Fr ~ 1.4-3.5 (Wohl and Ikeda, 1997; Finnegan et al., 2007; Johnson and Whipple, 2007, 2010). These previous studies showed that the erosional morphologies are not sensitive to the magnitude of the Fr number, although the Fr numbers in those experiments were greater than those around Fr = 1 (transcritical) that are thought to be typical in natural bedrock rivers, even at flood stage (Tinkler, 1997b; Tinkler and Wohl, 1998; Richardson and Carling, 2006; Johnson and Whipple, 2007). Our experiments are consistent with those results and demonstrate that even when the flow is subcritical (Fr < 1), erosional bedforms can still be generated by flume-scale experiments with analogue bedrock substrates. Lastly, the present experiments do not exhibit brittle fracturing unlike those experiments with concrete-based or rock substrates or natural bedrock channels (Johnson and Whipple, 2007; Wilson et al., 2013; Lamb et al., 2015), suggesting that brittle fracturing is not critical for the genesis of these erosive bedrock features.

Field studies of polished rock surfaces composed of erosive bedforms and sculpted by sediments have argued that these surfaces are dominated by suspension- rather than saltation-driven abrasion (Hancock et al., 1998; Whipple et al., 2000a). The present study provides support for these field studies and provides experimental confirmation of the importance of suspension-driven abrasion in the genesis and maintenance of sculpted surfaces of erosive bedforms.

Some previous experiments have concentrated on the effects of saltation-driven abrasion in order to answer a host of important questions, for example, the effects of varied bedload flux on the roughness of the bedrock substrate, incision rate, and channel morphology (Hancock et al., 1998; Finnegan et al., 2007). Furthermore, the numerical saltation-abrasion model (Sklar and Dietrich, 2004: Turowski et al., 2007) has been widely utilised to model bedrock river erosion from reach scales, through river profile development, to landscape evolution (e.g., Crosby et al., 2007; Cook et al., 2012; Egholm et al., 2013; Scheingross et al., 2014). However, there is increasing recognition that suspension-load abrasion is also important in many bedrock rivers and that a total-load model incorporating the effects of abrasion from saltation-load and suspension-load is required for more accurate modelling of many of these processes (e.g., Lamb et al., 2008; Scheingross et al., 2014). Despite this recognition that suspension-load is important across a wide range of problems such as bedload erosion rates, knickpoint dynamics, and slot canyons (Lamb et al., 2015), a number of issues with extending existing experimental approaches to the suspension-dominated abrasion regime still exist. Critically, the high tensile strengths of existing experimental substrates means that large particles are required for any abrasion to occur (diameter > 0.2 mm for a range of natural bedrock, as measured in a ball mill; Sklar and Dietrich, 2001, 2004), and these particles require correspondingly high flow velocities to be transported in the suspension regime. Additionally, even for larger particles erosion rates across existing experimental substrates such as weak concrete may be very low, restricting the utility of these experimental substrates because of the large timescales required for measurable erosion. The present experiments demonstrate a method for extending the range of conditions that can be studied experimentally within realistic timescales to this suspension-driven abrasion regime. The method presented herein thus opens the potential to examine the temporal evolution of erosive bedrock features, the coupled effects of macroscopic turbulence and bedform development, incision rate, and the interaction of multiple bedforms. In addition, this experimental approach enables study of the effects of incorporating suspension-load abrasion on landscape evolution, and to the development of total-load abrasion models incorporating suspension-load abrasion.

5. Conclusion

Our experiments produced bedforms with highly analogous morphology to natural field examples, even at a scale that is orders of magnitude smaller than some natural examples. The experiments have for the first time reproduced the majority of bedform types that have been shown to occur on planar surfaces in homogenous bedrock substrates. Consequently, the experiments reported herein reinforce field observations that such surfaces and their erosive bedforms are primarily the result of suspension-driven abrasion rather than bedload-driven, saltation-dominated abrasion. Our experiments also indicate that cavitation, dissolution, corrosion, plucking, and supercritical flow conditions are not necessarily required for the generation of these forms. Whilst the clay substrates used here do not exhibit brittle fracturing, experiments were able to reproduce a variety of erosive bedforms. The present work provides a viable approach for extending the physical modelling of saltation-driven abrasion to the suspension-dominated abrasion regime within realistic laboratory timescales. This approach using modelling clay thus opens up the potential to study the evolution and fluid-bedform coupling of these bedforms, as well as experimentally examine the influence of suspension-dominated abrasion on landscape evolution.

Acknowledgements

This research was supported by a Leeds-CSC Scholarship (CSC-UoL) and China Postdoctoral Science Foundation funded project (2015M581566). We are particularly grateful to Gareth Keevil and Russell Dixon at the Sorby Laboratory, University of Leeds, for their extensive help designing and preparing the experimental setup. We would especially like to thank Wayne Stephenson for constructive comments on an early version of this manuscript. We thank Vic Baker, Phairot Chatanantavet, and three other anonymous reviewers for their thorough and constructive comments that greatly improved this manuscript. We also thank journal editor Richard Marston for providing us with five excellent reviews of our manuscript.

References

Alexander, H.S., 1932. Pothole erosion. The Journal of Geology 40, 305-337.

Allen, J.R.L., 1969. Erosional current marks of weakly cohesive mud beds. Journal of Sedimentary Research 39(2), 607-623.

Allen, J.R.L., 1971. Transverse erosional marks of mud and rock: their physical basis and geological significance. Sedimentary Geology 5(3), 167-385.

Allen, J.R.L., 1982. Sedimentary structures: their character and physical basis, Volume 2. Elsevier Scientific, Amsterdam, 663 pp.

Ängeby, O., 1951. Pothole erosion in recent waterfalls. Lund Studies in Geography, Series A 2, 1-34.

Anton, L., Mather, A.E., Stokes, M., Muñoz-Martin, A., De Vicente, G., 2015. Exceptional river gorge formation from unexceptional floods. Nature Communications 6:7963, doi:10.1038/ncomms8963.

Baker, V.R., 1974. Erosional forms and processes for the catastrophic Pleistocene Missoula floods in eastern Washington. In: Morisawa, M. (Ed.,) Fluvial Geomorphology, Allen and Unwin, London, pp. 123-148.

Baker, V.R., 1978. Large-scale erosional and depositional features of the Channeled Scabland. In: Baker, V.R., Nummedal, D., (Eds.), The Channeled Scabland: National Aeronautics and Space Administration Planetary Geology Program, Washington, D.C., pp. 81-115.

Baker, V.R., 1979. Erosional processes in channelized water flows on Mars. Journal of Geophysical Research 84, 7985-7993.

Baker, V.R., Costa, J.E., 1987. Flood power. In: Mayer, L., Nash, D., (Eds.), Catastrophic Flooding, Allen and Unwin, Boston, pp. 1-21.

Baker, V.R., Kale, V.S., 1998. The role of extreme floods in shaping bedrock channels. In: Tinkler, K.J., Wohl, E.E. (Eds.), Rivers over Rock: Fluvial Processes in Bedrock Channels, American Geophysical Union Geophysical Monograph Series 107, pp. 153-166.

Baker, V.R., Komar, P., 1987. Columbia and Snake River Plains. In: Graf, W.L., (Ed.), Geomorphic systems of North America, Geological Society of America, The Geology of North America, Centennial Special, 2, pp. 403-468.

Baker, V.R., Milton, D.J., 1974. Erosion by catastrophic floods on Mars and Earth. Icarus 23, 27-41.

Baker, V.R., Pickup, G., 1987. Flood geomorphology of the Katherine Gorge, Northern Territory, Australia. Geological Society of America Bulletin 98(6), 635-646.

Best, J.L., Kirkbride, A.D., Peakall, J., 2001. Mean flow and turbulence structure of sediment-laden gravity currents: new insights using ultrasonic Doppler velocity profiling. In: McCaffrey, W.D., Kneller, B.C., Peakall, J. (Eds.), Particulate Gravity Currents. International Association of Sedimentology Special Publication 31, Blackwell Science, Oxford, pp. 159–172.

Büdel, J., 1982. Climatic geomorphology. Princeton, New Jersey, Princeton University Press, 443 pp. (Translation of Büdel, 1977, by L. Fischer and D. Busche.)

Carling, P.A., Herget, J., Lanz, J.K., Richardson, K., Pacifici, A., 2009. Channel-scale erosional bedforms in bedrock and in loose granular material: Character, processes and implications. In: Burr, D.M., Carling, P.A., Baker, V.R. (Eds.), Megaflooding on Earth and Mars, pp. 13-32.

Carter, C.L., Anderson, R.S., 2006. Fluvial erosion of physically modeled abrasion dominated slot canyons. Geomorphology 81, 89–113.

Chatanantavet, P., Parker, G., 2009. Physically based modeling of bedrock incision by abrasion, plucking, and macroabrasion. Journal of Geophysical Research: Earth Surface, 114, F04018, doi: 10.1029/2008JF001044.

Cook, K.L., Turowski, J.M., Hovius, N., 2012. A demonstration of the importance of bedload transport for fluvial bedrock erosion and knickpoint propagation. Earth Surface Processes and Landforms 38, 683–695.

Crosby, B.T., Whipple, K.X., Gasparini, N.M., Wobus, C.W., 2007. Formation of fluvial hanging valleys: Theory and simulation. Journal of Geophysical Research 112, F3, doi:10.1029/2006jf000566.

Davis, R.H., Rager, D.A., Good, B.T., 2002. Elastohydrodynamic rebound of spheres from coated surfaces. Journal of Fluid Mechanics 468, 107–119.

Dzulynski, S., 1965. New data on experimental production of sedimentary structures. Journal of Sedimentary Petrology 35, 196-212.

Dzulynski, S., 1996. Erosional and deformational structures in single sedimentary beds: a genetic commentary. Annals Societatis Geologorum Poloniae 66, 101-189.

Dzulynski, S., Sanders, J.E., 1962. Current marks on firm mud bottoms. Trans. of the Connecticut Academy of Arts and Sciences 42, 57-96.

Dzulynski, S., Walton, E.K., 1963. Experimental production of sole marking. Trans. of the Edinburgh Geological Society 19, 279-305.

Egholm, D., Knudsen, M., Sandiford, M., 2013. Lifespan of mountain ranges scaled by feedbacks between landsliding and erosion by rivers. Nature 498, 475–478.

Elston, E.D., 1917. Potholes: their variety, origin and significance. The Scientific Monthly 5, 554-567.

Elston, E.D., 1918. Potholes: their variety, origin and significance. II. The Scientific Monthly 6, 37-51.

Engel, P., 1976. Impact Wear of Materials. Elsevier Science Ltd, New York, pp 356.

Euler, T., Herget, J., 2012. Controls on local scour and deposition induced by obstacles in fluvial environments. Catena 91, 35-46.

Finnegan, N.J., Sklar, L.S., Fuller, T.K., 2007. Interplay of sediment supply, river incision, and channel morphology revealed by the transient evolution of an experimental bedrock channel. J. Geophys. Res. Earth Surf. 112 (F3), F03S11.

Gibbs, R.J., Matthews, M.D., Link, D.A., 1971. The relationship between sphere size and settling velocity. Journal of Sedimentary Petrology 41, 7-18.

Hancock, G.S., Anderson, R.S., Whipple, K.X., 1998. Beyond power: Bedrock river incision process and form. In: Tinkler, K.J., Wohl, E.E. (Eds.), Rivers over Rock: Fluvial Processes in Bedrock Channels, American Geophysical Union Geophysical Monograph Series 107, pp. 35-60.

Herget, J., 2005. Reconstruction of Pleistocene ice-dammed lake outburst floods in the Altai Mountains, Siberia. Geological Society of America Special Paper 386, 118 pp.

Herget, J., Eurler, T., Roggenkamp, T., Zemke, J, 2013. Obstacle marks as palaeohydraulic indicators in Pleistocene megafloods. Hydrology Research 44, 300-317.

Huang, W.H., Keller, W.D., 1971. Dissolution of clay minerals in dilute organic acids at room temperature. The American Mineralogist 56, 1082-1095.

Ives, R.L., 1948. Plunge pools, potholes, and related features. Rocks and Minerals 23(1), 3-10.

Jennings, J.N., 1983. Swirlholes and related bedrock river channel forms. The Australian Geographer 15(6), 411-414.

Johnson, J.P., Whipple, K.X., 2007. Feedbacks between erosion and sediment transport in experimental bedrock channels. Earth Surface Processes and Landforms 32, 1048-1062.

Johnson, J.P., Whipple, K.X., 2010. Evaluating the controls of shear stress, sediment supply, alluvial cover, and channel morphology on experimental bedrock incision rate. Journal of Geophysical Research: Earth Surface 115(F2), F02018.

Joseph, G.G., Zenit, R., Hunt, M.L., Rosenwinkel, A.M., 2001. Particle-wall collisions in a viscous fluid. Journal of Fluid Mechanics 433, 329–346.

King, P.B., 1927. Corrosion and Corrasion on Barton Creek, Austin, Texas. The Journal of Geology 35, 631-638.

Kor, P.S.G., Cowell, D.W., 1998. Evidence for catastrophic subglacial meltwater sheetflood events on the Bruce Peninsula, Ontario. Canadian Journal of Earth Sciences 35(10), 1180-1202.

Kor, P.S.G, Shaw, J., Sharpe, D.R., 1991. Erosion of bedrock by subglacial meltwater, Georgian Bay, Ontario. Canadian Journal of Earth Sciences 28, 623-642.

Lamb, M.P., Fonstad, M.A., 2010. Rapid formation of a modern bedrock canyon by a single flood event. Nature Geoscience 3 (7), 477–481.

Lamb, M.P., Dietrich, W.E., Sklar, L.S., 2008. A model for fluvial bedrock incision by impacting suspended and bed load sediment. Journal of Geophysical Research 113, doi:10.1029/2007JF000915.

Lamb, M.P., Finnegan, N.J., Scheingross, J.S., Sklar, L.S., 2015. New insights into the mechanics of fluvial bedrock erosion through flume experiments and theory. Geomorphology 244, 33-55, doi: 10.1016/j.geomorph.2015.03.003.

Li, X., Hunt, M.L., Colonius, T., 2012. A contact model for normal immersed collisions between a particle and a wall. Journal of Fluid Mechanics 691, 123–145.

Lorenc, M.W., Barco, P.M., Saavedra, J., 1994. The evolution of potholes in granite bedrock, W Spain. Catena 22(4), 265-274.

Lowe, D. R., 1979. Sediment gravity flows: their classification and some problems of application to natural flows and deposits. In: Doyle, L.J., Pilkey, O.H. (Eds.), Geology of Continental Slopes, SEPM Special publication 27, pp. 75-82.

Martini, I.P., Baker, V.R., Garzón, G., 2009. Flood and Megaflood Processes and Deposits: Recent and Ancient Examples. Special Publication of the IAS (32)17, John Wiley & Sons, 320 pp.

Maxson, J.H., Campbell, I., 1935. Stream fluting and stream erosion. The Journal of Geology 43, 729-744.

Munro-Stasiuk, M.J., Shaw, J., Sjogren, D.B., Brennand, T.A., Fisher, T.G., Sharpe, D.R., Kor, P.S.G., Beaney, C.L., Rains, B.B., 2009. The morphology and sedimentology of landforms created by subglacial megafloods. In: Burr, D.M., Carling, P.A., Baker, V.R. (Eds.), Megaflooding on Earth and Mars: Cambridge University Press, Cambridge, pp. 78-103.

Peakall, J., Ashworth, P., Best, J., 1996. Physical modelling in fluvial geomorphology: Principles, applications and unresolved issues. In: Rhoads, B.L., Thorn, C.E. (Eds.), The Scientific Nature of Geomorphology. John Wiley and Sons, Chichester, pp. 221-253.

Pelletier, J.D., Baker, V.R., 2011. The role of weathering in the formation of bedrock valleys on Earth and Mars: a numerical modeling study. Journal of Geophysical Research 116, E11007, doi:10.1029/2011JE003.

Richardson, K., Carling, P.A., 2005. A Typology of Sculpted Forms in Open Bedrock Channels. Geological Society of America Special Paper 392, pp. 108.

Richardson, K., Carling, P.A., 2006. The hydraulics of a straight bedrock channel: Insights from solute dispersion studies. Geomorphology 82, 98-125.

Ruiz-Angulo, A., Hunt, M.L., 2010. Measurements of the coefficient of restitution for particle collisions with ductile surfaces in a liquid. Granular_Matter 12, 185–191.

Scheingross et al., J.S., Brun, F., Lo, D.Y., Omerdin, K., Lamb, M.P., 2014. Experimental evidence for fluvial bedrock incision by suspended and bedload sediment. Geology 42, 523-526.

Sharpe, D.R., Shaw, J., 1989. Erosion of bedrock by subglacial meltwater, Cantley, Quebec. Geological Society of America Bulletin 101, 1011-1020.

Shepherd, R.G., Schumm, S.A., 1974. Experimental study of river incision. Geological Society of America Bulletin 85, 257–268.

Simpson, R.L. 2001. Junction Flows. Annual Review of Fluid Mechanics 33, 415–43.

Sjogren, D.B., Rains, R.B., 1995. Glaciofluvial erosion morphology and sediments of the Coronation-Spondin Scabland, east-central Alberta. Canadian Journal of Earth Sciences 32, 565-578.

Sklar, L.S., Dietrich, W.E., 2001. Sediment and rock strength controls on river incision into bedrock. Geology 29(12), 1087-1090.

Sklar, L.S., Dietrich, W.E., 2004. A mechanistic model for river incision into bedrock by saltating bed load. Water Resources Research 40(6), W06301.

Tinkler, K.J., 1993. Fluvially sculpted rock bedforms in Twenty Mile Creek, Niagara Peninsula, Ontario. Canadian Journal of Earth Sciences 30(5), 945-953.

Tinkler, K.J., 1997a. Rockbed wear at a flow convergence zone in Fifteen Mile Creek, Niagara Peninsula, Ontario. The Journal of Geology 105(2), 263-274.

Tinkler, K.J., 1997b. Critical flow in rockbed streams with estimated values for Manning's n. Geomorphology 20, 147-164.

Tinkler, K.J., Wohl, E.E., 1998. A primer on bedrock channels. In: Tinkler, K.J., Wohl, E.E. (Eds.), Rivers over Rock: Fluvial Processes in Bedrock Channels, American Geophysical Union Geophysical Monograph Series 107, pp. 1-18.

Turowski, J.M., Lague, D., Hovius, N., 2007. Cover effect in bedrock abrasion: A new derivation and its implications for the modeling of bedrock channel morphology. Journal of Geophysical Research 112, doi:10.1029/2006JF000697.

Whipple, K.X., Hancock, G.S., Anderson, R.S., 2000a. River incision into bedrock: Mechanics and relative efficacy of plucking, abrasion, and cavitation. Geological Society of America Bulletin 112(3), 490-503.

Whipple, K.X., Snyder, N.P., Dollenmayer, K., 2000b. Rates and processes of bedrock incision by the Upper Ukak River since the 1912 Novarupta ash flow in the Valley of Ten Thousand Smokes, Alaska. Geology 28(9), 835-838.

Wiberg, P., Smith, J., 1985. A theoretical model for saltating grains in water. Journal of Geophysical Research 90, 7341-7354.

Wilson, A., Lavé, J., 2014. Convergent evolution of abrading flow obstacles: Insights from analogue modelling of fluvial bedrock abrasion by coarse bedload. Geomorphology 208, 207-224.

Wilson, A., Hovius, N., Turowski, J.M., 2013. Upstream-facing convex surfaces: Bedrock bedforms produced by fluvial bedload abrasion. Geomorphology 180-181, 187-204.

Wohl, E.E., 1992. Bedrock benches and boulder bars: Floods in the Burdekin Gorge of Australia. Geological Society of America Bulletin 104(6), 770-778.

Wohl, E.E., 1993. Bedrock channel incision along Piccaninny Creek, Australia. The Journal of Geology 749-761.

Wohl, E.E., 1998. Bedrock channel morphology in relation to erosional processes. In: Tinkler, K.J., Wohl, E.E. (Eds.), Rivers over Rock: Fluvial Processes in Bedrock Channels, American Geophysical Union Geophysical Monograph Series 107, pp. 133-152.

Wohl, E.E., Achyuthan, H., 2002. Substrate influences on incised-channel morphology. The Journal of Geology 110(1), 115-120.

Wohl, E., Ikeda, H., 1997. Experimental simulation of channel incision into a cohesive substrate at varying gradients. Geology 25, 295–298.

Wohl, E.E., Ikeda, H., 1998. Patterns of bedrock channel erosion on the Boso Peninsula, Japan. Journal of Geology 106(3), 331-345.

Yin, D., 2013. Genesis and Evolution of Bedforms on Cohesive Mud Beds and Simulated Bedrock Channels. PhD thesis, University of Leeds, UK, pp. 309.

Zen, E., Prestegaard, K.L., 1994. Possible hydraulic significance of two kinds of potholes: Examples from the paleo-Potomac River. Geology 22(1), 47-50.

Appendix

Appendix 1. Bedform types and dimensions observed in the present experiments, and comparison with those described by (Richardson and Carling, 2005). **Remarks indicate which experiment features observed from.**

	Types of bedforms	Rock type	Length (cm)	Width (cm) (lower parts)	Depth (cm)	Remarks
Pothole	Ovoid pothole	Fine-grained sandstone	0.85 1.27	1.20 1.35	1.08 1.61	Fig. 4: A1-Exp. 2 : A2-Exp. 2
	Spiral-furrowed pothole	Microgranite	4.96 2.69	2.92 3.52	2.21 2.45	Exp. 1 Exp. 2
	Incipient pothole	Limestone	-	-	-	-
	Pothole with entry furrow	Calcareous mudstone	2.67 3.96	1.29 1.31	0.96 2.20	Fig. 4: D1-Exp. 2 : D2-Exp. 2
	Pothole with extended	Granitic gneiss	3.69	0.81	1.60	Fig. 4: B1-Exp. 2

exit furrow		3.31	1.06	1.60	: B3-Exp. 2
Open pothole	Fine- grained sandstone	2.41	1.54	2.71	Fig. 4: C1-Exp. 2
A pothole with horizontal furrows	Calcareous mudstone	-	-	-	-
Hierarchical pothole	Granitic gneiss	5.03 3.82	4.38 3.03	2.55 2.33	Exp. 1 Exp. 3
Convoluted pothole	Gneiss	9.46 1.73	5.92 1.25	2.76 1.04	Exp. 1 Exp. 3
Large isolated breached pothole	Granitic gneiss	-	-	-	-
Coalesced potholes	Granitic gneiss	-	-	-	-
Natural arch	Granitic gneiss	-	-	-	-
Natural pillar	Granitic gneiss	-	-	-	-
Closed lateral pothole	Granitic gneiss	-	-	-	-
Lateral pothole	Granitic gneiss	-	-	-	-
Conjugate linear lateral potholes	Granitic gneiss	-	-	-	-

	Compound lateral pothole of the hierarchical variety	Granitic gneiss	-	-	-	-
	Paired lateral potholes	Dolomit	-	-	-	-
Flute	Broad flute	Limestone	0.94	2.75	0.59	Exp. 2
	Narrow flute	Granitic gneiss	1.56	0.79	0.56	Exp. 2
	Flute with median ridge and internal secondary structures	Calcareous mudstone	2.65	1.47	1.07	Exp. 2
	Spindle-shaped flute	Rhyolitic agglomerate	2.62	0.65	0.59	Exp. 2
	Flute with internal secondary structures	Calcareous mudstone	2.41	1.44	1.43	Fig. 5: A1-Exp. 1
			3.09	2.49	0.69	: B1-Exp. 2
			2.71	1.34	0.47	: B2-Exp. 2
	Flute with external secondary structures	Limestone	6.38	1.41	0.65	Fig. 5: C1-Exp. 2
			3.99	1.33	0.84	: C2-Exp. 2
			7.88	2.44	0.71	: C3-Exp. 2
			3.01	1.14	1.25	: C4-Exp. 3
	En echelon flutes	Granitic gneiss	4.75	4.15	1.28	Exp. 2

	Paired flutes	Granitic gneiss	2.89	2.07	1.24	Exp. 1
	Lineations	Limestone	8.06	9.01	0.10	Exp. 2
Furrow	Straight short furrow	Limestone	2.09 2.52	0.82 0.80	1.50 0.99	Fig. 6: A1-Exp. 1 : A3-Exp. 2
	Curved short furrow	Calcareous mudstone	2.87	0.63	1.55	Exp. 2
	Cuspate, deep short furrow	Gneiss	2.09 2.52	0.82 0.80	1.50 0.99	Fig. 6: A1-Exp. 1 : A3-Exp. 2
	Paired short furrows	Calcareous mudstone	-	-	-	-
	Short furrow with internal secondary structures	Gneiss	-	-	-	-
	Straight parallel-sided furrow	Fine-grained sandstone	2.81	0.51	1.24	Exp. 2
	Curved parallel-sided furrow	Granitic gneiss	3.91	0.35	1.22	Exp. 2
	Sinuous parallel-sided furrow	Fine-grained sandstone	1.29 3.61 16.22	0.54 0.31 0.90	1.19 1.22 1.90	Fig. 6: B1-Exp. 3 : B3-Exp. 2 : B4-Exp. 1

Parallel-sided furrow with levees	Fine-grained sandstone	-	-	-	-
Chute furrow	Limestone	-	-	-	-
Chimney furrow	Interbedded limestone and marl	-	-	-	-
Bifurcating furrows	Microgranite	4.71 23.11	2.68 1.45 (bifurcating point)	1.50 1.50	Exp. 2 Exp. 3
Group of parallel-sided furrows	Limestone	2.20 (average)	0.68 (average)	0.76 (average)	Exp. 2
Regular compound parallel-sided furrows	Andesite	10.24	0.98	1.90	Exp. 2
Irregular compound parallel-sided furrows	Limestone	10.62 10.52	0.37 0.61	1.22 1.34	Exp. 2
Funnel-shaped furrow (underwater)	Medium-grained sandstone	2.44	1.62	0.56	Exp. 2
Bulbous furrow (underwater)	Fine-grained sandstone	3.28	1.55	1.10	Exp. 2

	Runnel with cusped margins	Fine-grained sandstone	-	-	-	-
	Oblique sloping furrows	Granitic gneiss	-	-	-	-
	Compound transverse furrows	Fine-grained sandstone	-	-	-	-
	Cross-channel furrow (underwater).	Fine-grained sandstone	-	-	-	-
	Straight reversed furrow	Granitic gneiss	-	-	-	-
	Curved reversed furrow	Granitic gneiss	4.02	0.61	2.00	Exp. 3
	Open-ended reversed furrow	Granitic gneiss	5.79	4.07	2.08	Exp. 1
	Branched reversed furrow	Granitic gneiss	-	-	-	-
	Group of parallel reversed furrows	Granitic gneiss	3.28	2.78	1.68	Exp. 1
Convex and undulating surfaces	Convergent furrow complex	Granitic gneiss	6.66	1.96	1.08	Exp. 2
	Yin- yang furrow	Calcareous mudstone	-	-	-	-

complex					
Nested curved furrow complex	Medium-grained sandstone	-	-	-	-
Overhanging concave surface	Granitic gneiss	-	-	-	-
Cavetto	Limestone	-	-	-	-
Taffoni	Fine-grained sandstone	-	-	-	-
Shallow concave surfaces	Calcareous mudstone	-	-	-	-
Hummocky forms	Limestone	13.25	3.50	0.59	Fig. 7: A1-Exp. 2
Pseudoripples	Andesite	-	-	-	-
Microripples	Gneiss	-	-	-	-
Partially abraded surface	Limestone	-	-	-	-
Bladed forms	Calcareous mudstone	3.31 7.40	1.93 0.97	0.74 1.60	Exp. 2
Obstacle mark (Current crescents with	Rhyolitic agglomerate	3.12 2.72	2.38 (0.79) 1.746 (0.47)	1.84 1.69	Fig. 7: B1-Exp. 1 : B2-Exp. 1

secondary sculpting)		2.33	2.99 (0.76)	1.66	: B3-Exp. 2
Pseudoripples with short furrows	Andesite	-	-	-	-
Runnel with SCHF	Gneiss	-	-	-	-
Parallel runnels with step-pool structures	Granite	-	-	-	-
High relief Hummocky forms with current crescents	Limestone	-	-	-	-
Hummocky forms with steep lee faces	Limestone	-	-	-	-